


# Anomalous layer-dependent photoluminescence spectra of supertwisted spiral WS<sub>2</sub>

MINRU QI,<sup>1</sup> TONG TONG,<sup>2</sup> XIAOPENG FAN,<sup>2,4</sup> XIANGDONG LI,<sup>1</sup>  
SHEN WANG,<sup>3</sup> GUOFENG ZHANG,<sup>1</sup> RUIYUN CHEN,<sup>1</sup>  JIANYONG  
HU,<sup>1</sup> ZHICHUN YANG,<sup>1</sup> GANYING ZENG,<sup>1</sup>  CHENGBING QIN,<sup>1,2,5</sup>   
LIANTUAN XIAO,<sup>1,2,6</sup> AND SUOTANG JIA<sup>1</sup>

<sup>1</sup>State Key Laboratory of Quantum Optics and Quantum Optics Devices, Institute of Laser Spectroscopy, Collaborative Innovation Center of Extreme Optics, Shanxi University, Taiyuan, Shanxi 030006, China

<sup>2</sup>College of Physics, Taiyuan University of Technology, Taiyuan, 030024, China

<sup>3</sup>College of Physics and Electronic Engineering, Shanxi University, Taiyuan, Shanxi 030006, China

<sup>4</sup>xiaopengfan@tyut.edu.cn

<sup>5</sup>chbqin@sxu.edu.cn

<sup>6</sup>xt@sxu.edu.cn

**Abstract:** Twisted stacking of two-dimensional materials with broken inversion symmetry, such as spiral MoTe<sub>2</sub> nanopylamids and supertwisted spiral WS<sub>2</sub>, emerge extremely strong second- and third-harmonic generation. Unlike well-studied nonlinear optical effects in these newly synthesized layered materials, photoluminescence (PL) spectra and exciton information involving their optoelectronic applications remain unknown. Here, we report layer- and power-dependent PL spectra of the supertwisted spiral WS<sub>2</sub>. The anomalous layer-dependent PL evolutions that PL intensity almost linearly increases with the rise of layer thickness have been determined. Furthermore, from the power-dependent spectra, we find the power exponents of the supertwisted spiral WS<sub>2</sub> are smaller than 1, while those of the conventional multilayer WS<sub>2</sub> are bigger than 1. These two abnormal phenomena indicate the enlarged interlayer spacing and the decoupling interlayer interaction in the supertwisted spiral WS<sub>2</sub>. These observations provide insight into PL features in the supertwisted spiral materials and may pave the way for further optoelectronic devices based on the twisted stacking materials.

© 2024 Optica Publishing Group under the terms of the [Optica Open Access Publishing Agreement](#)

## 1. Introduction

Atomically thin two-dimensional (2D) transition metal dichalcogenides (TMDCs) with the chemical formula MX<sub>2</sub> (M = Mo, W, and X = S, Se) have attracted great interest, due to their unique electric and optical properties [1,2], such as reduced dielectric screening [3], tunable optical bandgap [4], large binding energy [5], strong spin-orbit coupling [6], spin and valley degrees [7]. The promising applications of these layered materials in electronic and optoelectronics, including phototransistors [8], photodetectors [9], light-emitting devices [10], and solar cells [11], have been extensively explored in recent years. One of the unique properties of TMDCs is their layer-dependent features, which will undergo remarkable changes in the electronic structures and optical performance depending on the number of layers. For example, TMDCs will evolve from an indirect-band gap to a direct-band gap when the number of layers decreases to a monolayer, which results in strong photoluminescence (PL) for the monolayer materials [12]. Accordingly, the multilayer TMDCs typically emerge with reduced optical features and fragile PL intensity [12,13]. However, for some practical applications (such as nonlinear optics), multilayer TMDCs are highly desired because of the limited light-matter interaction at atomic thickness [14–16]. Two predominant solutions are widely used: improving the features by external stimuli (including chemical/electric doping [17,18], defect engineering [19,20], and

plasmonic enhancement [21,22]) and fabricating new layered materials with specific atomic structures that suppress or even eliminate the layer-dependent properties.

Very recently, spiral nanosheets or nanopyramids, representative of new layered materials with specific atomic structures [23–25], have been successfully fabricated by chemical vapor deposition. Experimental results have demonstrated that the strong nonlinear optical effects (including second- and third-harmonic generation) emerge in these spiral structures [26,27], where the intensity of the second-harmonic generation quadratically increases with the layer numbers, rather than diminishes the oscillation of 2H stacking TMDCs [24]. The nonlinear susceptibility of the spiral structures is estimated to be around 1-2 orders of magnitude larger than those conventionally reported TMDCs [24]. This enhancement is mainly enabled by their broken inversion symmetry, weak interlayer coupling, and strong light-matter interaction. Analogous to the spiral TMDCs, the supertwisted spirals are another representative layered material [28–31]. The growing model of the supertwisted spiral has been described as the growth of layered materials with screw-dislocation spirals on non-Euclidean surfaces (such as TMDCs draped over nanoparticles near the centers of the spirals), leading to continuously twisted multilayer superstructures [28]. The second harmonic generation and the rotational symmetry of the supertwisted WS<sub>2</sub> have also been investigated [32]. Unlike well-studied nonlinear optical effects, little is known about the PL properties of supertwisted spiral layered materials, which is of great importance for their optoelectronic applications.

In this work, we produced the supertwisted spiral WS<sub>2</sub> by chemical vapor deposition and investigated their layer-dependent and power-dependent PL spectra. The optical features, including PL intensity, photon energy of the neutral and charged excitons, and the power exponents of the supertwisted spiral WS<sub>2</sub>, have been determined and compared with the conventional multilayer WS<sub>2</sub>, synchronously growth on the substrate around the spiral WS<sub>2</sub>. The anomalous layer-dependent PL intensity that increases with the lift of the layer thickness has been observed. This novel property eliminates the PL decay in conventional multilayer TMDCs, and may offer new opportunities to fabricate high-quality optoelectronic devices with thick layered materials.

## 2. Experiment

Optical experiments were conducted at room temperature using a homemade scanning confocal microscope testing system. The experimental schematic, which can also be found in the [Supplement 1](#) (Fig. S3), has been described in detail elsewhere. Particularly, a 532 nm continuum-wave (CW) laser was used as the excitation source to perform layer-dependent and power-dependent PL spectra. The laser was collimated by a beam expander (BE) and filtered by a band-pass filter (BFP, Semrock, LL01-532-12.5). After being reflected by a dichroic mirror (DM, Semrock, Di01-R532-25 × 36), the laser was focused by a dry objective (100×, NA = 0.9, NIRLT-APO, Attocube). The supertwisted spiral WS<sub>2</sub> was placed on a motorized three-dimensional piezoelectric translation nano-stage (PZT, nanoFaktur, PXY 102 CAP) with typical repeatability of less than 35 nm. The high spatial resolution guarantees that the laser spots can be located at specific positions on the different layers. PL intensity was collected by using the same objective. After passing through the D and a long-pass filter (570LP) to block the back-scattered laser and the background noise, PL was further filtered spatially using a 100 μm pinhole and analyzed by a spectrometer (Andor, SR500I-A) with a cooled charge-coupled device (CCD, Andor, DR-316B-LDC-DD).

The optical image of the supertwisted spiral WS<sub>2</sub> was captured by optical microscopy (OLYMPUS TH4-200). The morphology of the sample was characterized by atomic force microscopy (AFM, Flex-Axi). Raman spectroscopy was performed using a commercial Raman spectrometer (LabRAM HR, Horiba) using the 532 nm laser excitation.

### 3. Results and discussion

The supertwisted spiral WS<sub>2</sub> used in this experiment was produced by chemical vapor deposition (CVD) growth on a non-Euclidean substrate (cone surface) using screw-dislocation-driven growth techniques [27]. The details of the production can be found in previous works [23]. Non-protrusions were specially introduced during the preparation. Thus, we proposed that some nanoparticles (such as the nucleates or nanocrystals of W) occasionally serve as the protrusion, leading to the spontaneous growth of the supertwisted spiral structures. In this case, the supertwisted spiral WS<sub>2</sub> is low-yield and randomly distributed on the substrate among other structures of layered WS<sub>2</sub> (such as film, multilayer triangular nanosheets, and aligned spirals). As the optical image shown in Fig. 1(a), a supertwisted spiral structure can be clearly determined, with near three-fold symmetric and clockwise-like screw rise. The morphology of the supertwisted spiral WS<sub>2</sub> has also been characterized by atomic force microscopy (AFM), as the image presented in Fig. 1(b). Normally, the lateral size of the entire spiral structure is less than 10 μm, and that of each successive layer ranges from about 2 μm to less than 1 μm, from the edge to the center. The twist angle,  $\alpha$ , between successive layers of this spiral WS<sub>2</sub> is about 13°. We also prepared the supertwisted spiral WS<sub>2</sub> with different twist angles in the experiment, as Fig. S1 shown in the [Supplement 1](#). The thicknesses of the successive layers are also determined by AFM; the results are displayed in Fig. 1(d). For the sake of simplicity, if not explicitly mentioned, the three-fold-like structures are named the upper, left, and bottom petals, and shorted as U, L, and B, respectively (Fig. 1(c)). It can be found that the thicknesses of each layer on the three petals are similar, proving the excellent quality of the supertwisted spiral structures. Note that the thickness of the outside (*i.e.*, 1<sup>st</sup> layer) is about 0.77 nm, consistent with that of the conventional monolayer WS<sub>2</sub> [33]. In contrast, the thickness difference between the 4<sup>th</sup> and 5<sup>th</sup> layers is about 1.71 nm, indicating the possibility of an enlarged interlayer spacing and overlapping two dislocations [29,34]. We further characterized the supertwisted WS<sub>2</sub> using Raman spectroscopy, as shown in Fig. 1(e). Two strong and distinct peaks can be found at 350.6 cm<sup>-1</sup> and 420.3 cm<sup>-1</sup>, which can undoubtedly be attributed to in-plane  $E_{2g}^1$  and out-of-plane  $A_{1g}$  modes, respectively. Compared to conventional monolayer WS<sub>2</sub> [35,36], the out-of-plane mode presents a significant blue shift, indicating the multilayer features of the spiral WS<sub>2</sub> and the possible interlayer coupling. This result is also consistent with previous reports.

Understanding the spectral features of nanomaterials is crucial for their optical and optoelectronic applications. However, to our knowledge, PL spectra and the corresponding exciton information of the supertwisted spiral WS<sub>2</sub> remain unclear. Thus, we performed layer-dependent and power-dependent PL spectra of the supertwisted spiral WS<sub>2</sub> under the excitation of a 532 nm continuous-wave laser, to comprehensively explore their optical features. Figure 1(f) presents the PL spectra of the bottom petal (abbreviated as B) in the supertwisted spiral WS<sub>2</sub>. As expected, PL spectra show two distinct peaks in the region of 1.2 eV to 2.2 eV, where the high-energy peak (~1.95 eV) is usually attributed to the direct band transition (marked as X), while the low-energy peak (~1.45 eV) can be classified as the indirect band transition (marked as I). This phenomenon agrees well with the previous reports [37]. Second, and in particular, with the increase of the layer thickness, the PL intensity of the direct band transition of the supertwisted spiral WS<sub>2</sub> constantly lifts, while their peak position shows ignorable change. This anomalous PL enhancement is quite different from conventional TMDCs, where PL intensities generally decline with the increase of layer number [12,38,39]. Last, the PL intensities of the indirect band transitions display insignificant change, as the inset shown in Fig. 1(f).

To explore the underlying mechanism of unique spectral evolution shown in Fig. 1(f), we fitted the direct band transition of the supertwisted spiral WS<sub>2</sub> with two Gauss functions and compared them with the other multilayer (ML) WS<sub>2</sub> nanosheets, as illustrated in Fig. 2. Generally, these two peaks can be attributed to the neutral ( $X^0$ , ~2.0 eV) and charged exciton ( $X^-$ , ~1.95 eV), respectively. As shown in Figs. 2(g) and 2(h), the photon energy and the spectral width of the

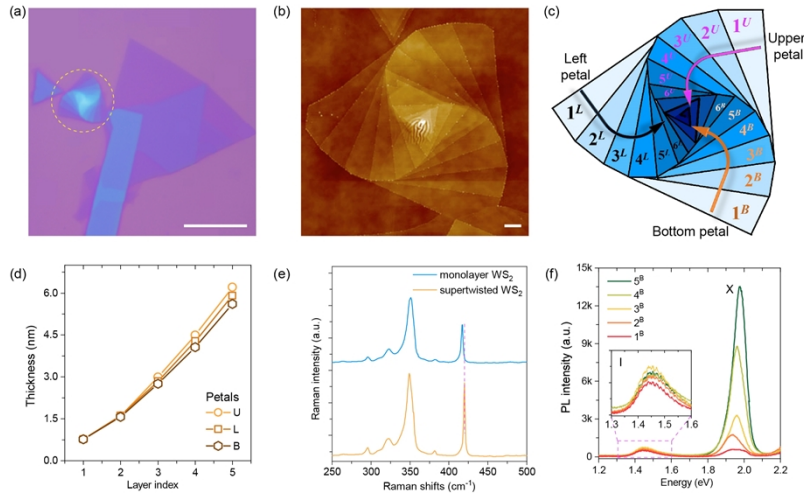


**Fig. 1.** Characterization of the supertwisted spiral  $\text{WS}_2$ . (a) The optical microscopy image of the prepared sample, the supertwisted spiral  $\text{WS}_2$  has been highlighted by the dashed circle. Scale bar:  $10\ \mu\text{m}$ . (b) Atomic force microscopy image of the supertwisted spiral  $\text{WS}_2$ . Scale bar:  $1\ \mu\text{m}$ . (c) Schematic illustration of the three-fold-like structures, which are named the upper, left, and bottom petals. The layer indexes have also been marked. (d) The thickness of the first five successive layers for the three petals. (e) Raman spectra of the supertwisted spiral  $\text{WS}_2$  and conventional monolayer  $\text{WS}_2$ , respectively. The excitation source was a  $532\ \text{nm}$  continuous-wave laser. The dashed line at  $419\ \text{cm}^{-1}$  is provided to guide the eye. (f) Photoluminescence (PL) spectra of the bottom petal, the high- and low-energy peaks are assigned as the direct band (marked as X) and indirect band transitions (marked as I). The inset shows the enlarged region of the indirect band transition.

two excitons as a function of layer thickness present subtle shifts, except for the PL spectra of the second successive layer (noted as  $2^{\text{B}}$ ). We will show that the energy difference between the first and second successive layers for the up and left petals ( $1^{\text{U}}$  and  $2^{\text{U}}$ ,  $1^{\text{L}}$  and  $2^{\text{L}}$ ) is also pronounced, as illustrated in Fig. 4. These variations indicate that the interlayer coupling and thus the optical properties of the first two layers are sensitive to their thickness. For even thicker layers (such as  $3^{\text{B}}$  to  $5^{\text{B}}$ ), these variations are neglected. The broader spectral width for the  $2^{\text{B}}$  layer may be attributed to the unpredictable defect and impurity in the measured areas. On the other hand, PL intensities linearly increased with the lift of the layer thickness, as the solid fit line shown in Fig. 2(i). Furthermore, the analysis also uncovers that the spectral weight of neutral excitons increases for the first three layers and then stands at a plateau level, as illustrated in Fig. 2(j). For comparison, we also conducted PL spectra of  $\text{WS}_2$  with other multilayer structures, surrounding the supertwisted spiral  $\text{WS}_2$ , as shown in Fig. 2(a). These multilayer nanosheets are preparation synchronous through CVD method while forming diverse structures due to different growth mechanism. To simplify, we marked these multilayer nanosheets from the thinnest to the thickest layer as  $1^{\text{st}}$  to  $5^{\text{th}}$ , as illustrated in Fig. 2(a). Note that the  $1^{\text{st}}$  layer is not monolayer (the thickness of which is about  $1.5\ \text{nm}$ ). PL spectra of these nanosheets and their analysis are presented in Figs. 2(k) to 2(o), respectively. First, we can note that the full widths at half maximum (FWHM) of both neutral and charged excitons are broader than that of the supertwisted spiral  $\text{WS}_2$ , as summarized in Fig. 2(h). Second, with the increase of the layer thickness, PL intensities show slight decline rather than significant rise. Interestingly, even for the similar thickness in the two kinds of structures (such as  $5^{\text{B}}$  with  $7.9\ \text{nm}$  vs.  $5^{\text{th}}$  with  $8.2\ \text{nm}$ ), PL intensity of  $5^{\text{B}}$  in the supertwisted spiral  $\text{WS}_2$  is almost 15 folds stronger than the  $5^{\text{th}}$  layer in the conventional

WS<sub>2</sub>. This enhanced light-matter interaction in the supertwisted spiral WS<sub>2</sub> makes potential applications that only emerge in bulk materials, such as laser emission and strong coupling between photons and excitons [40–42]. Third, in these multilayer nanosheets, the charged exciton predominates PL intensity, indicating heavy doping electrons arising from surface defects or substrate effects [43]. This phenomenon might originate from their large surface, compared to the small surface of the supertwisted spiral WS<sub>2</sub>. Lastly, from the fitting results, we can also find that the photon energy of the neutral exciton presents a significant blueshift with the increase of the layer thickness. The underlying mechanism is still inconclusively explained and needs further work.

We also investigated the excitation power dependence of the PL spectra for the supertwisted spiral WS<sub>2</sub>. The results of the bottom petal are shown in Fig. 3. As expected, PL intensities of the spiral WS<sub>2</sub> (the 2<sup>B</sup> layer in Fig. 3(a)) increased with the increasing excitation power in the range of 50 μW to 400 μW, and some saturation phenomena can be determined when the excitation power increases further. However, for the enlarged excitation power, the spiral WS<sub>2</sub> may be broken. Thus, we kept the maximum excitation power at 400 μW in the experiment. The power dependence PL intensities ( $I$ ) can be fitted by the power law equation,  $I = a \times P^n$ , where  $P$  represents the excitation power. The fitting results of different layers in the spiral WS<sub>2</sub> are presented in Fig. 3(g), with the exponent  $n$  ranging from  $0.81 \pm 0.05$  to  $0.90 \pm 0.10$ , in reasonable agreement with the linear behavior. We also fitted the power-dependent PL spectra with two Gauss functions to further understand their power-dependent optical features. Figures 3(b) and 3(c) present the fit results for the excitation powers of 50 μW and 400 μW, respectively. Note that photon energies of both X<sup>0</sup> and X<sup>-</sup> excitons manifest a continuous red-shift with the increase of the excitation power, as presented in Fig. 3(d). This result may be attributed to the rise in carriers density and thus the band structure renormalization, as reported in the previous works [44]. Interestingly, the trion dissociation energy,  $\Delta E$  (*i.e.*, the energy difference between X<sup>0</sup> and X<sup>-</sup> excitons) [45], as a function of excitation power for different layers in the spiral WS<sub>2</sub> presents distinct behavior, as shown in Fig. 3(e). For example, the trion dissociation energy in the 1<sup>B</sup> layer shows a slight increase (from 35.0 meV to 38.4 meV, as depicted in Fig. 3(e)<sub>1</sub>), while that in the 3<sup>B</sup> layer shows a significant decrease (from 58.8 meV to 46.0 meV, as illustrated in Fig. 3(e)<sub>3</sub>). Contrasting these, the spectral weight of X<sup>0</sup> and X<sup>-</sup> excitons for different layers (except the 4<sup>B</sup> layer) exhibit similar behavior. These phenomena indicate the diverse interaction in separate layers and prove that the supertwisted spiral WS<sub>2</sub> can offer a facile and versatile platform for the exploration of low-dimensional physics. For comparison, power-dependent PL spectra of conventional multilayer WS<sub>2</sub> have also been performed, as shown in Fig. 3(f). Spectral analysis determined that the photon energy of the charged exciton also manifests a continuous red-shift with the increase of the excitation power, while that of the neutral exciton presents ignorable variation (Fig. S2 in Supplement 1). What's more, the power law fits of the multilayer WS<sub>2</sub> show quite different behaviors compared to the spiral WS<sub>2</sub> (as illustrated in Figs. 3(g) and 3(h)), with the power exponents ranging from 1.19 to 1.42 (Fig. 4(e)<sub>1</sub>). These distinctions further reveal the unique optical properties of the supertwisted spiral WS<sub>2</sub>.

The PL spectra of the upper and left petals are also performed to illustrate the versatile features of the spiral WS<sub>2</sub>, as presented in Fig. 4. Note that the PL spectrum of the 1<sup>U</sup> layer exhibits a broad width, where the photon energy of the charged exciton is much lower than other layers, as presented in Fig. 4(d). This result hints strong substrate effects in this layer, such as heavy doping electrons. The substrate effect combined with interlayer coupling also leads to insignificant variations in the PL intensities of the 1<sup>U</sup> to 3<sup>U</sup> layers. Even so, the unique rule that PL intensity almost increases linearly with the lift of the thickness in the supertwisted spiral WS<sub>2</sub> remains active, as shown in Figs. 4(b) and 4(c). We speculate that the increased PL intensity can be attributed to the enlarged interlayer (Fig. 1(d)) spacing and the interlayer decoupling. Thus, the total PL intensity of the thick layers (such as the 5<sup>U</sup> and 5L layers) can be treated as the

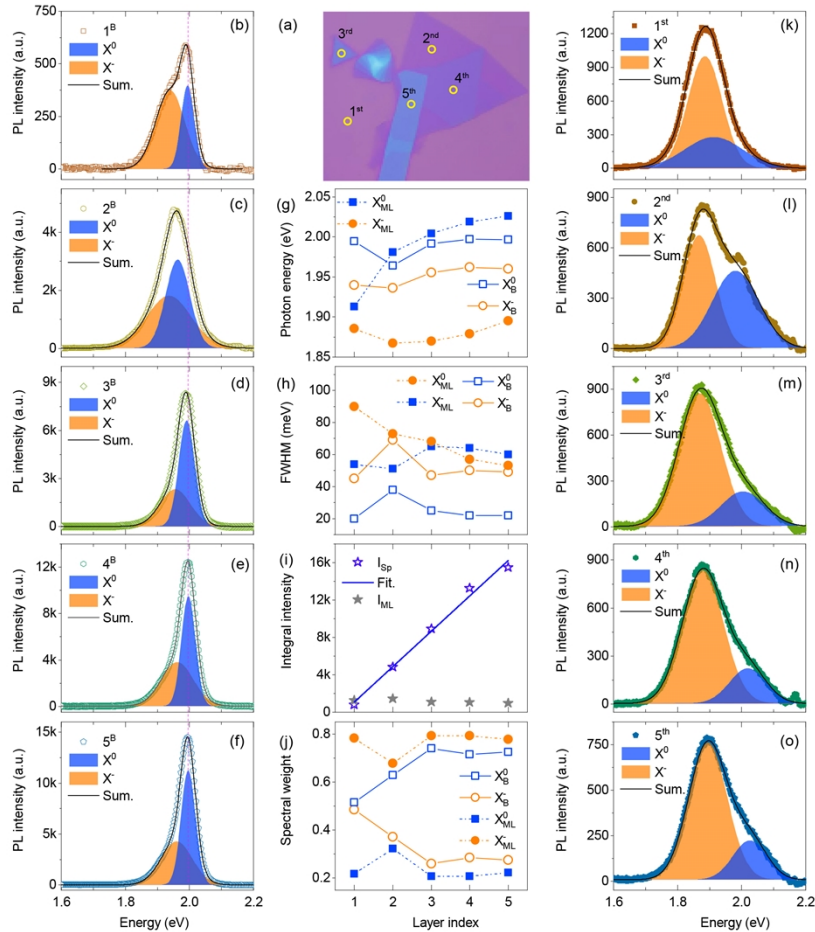


**Fig. 2.** Layer-dependent PL spectra of the supertwisted spiral WS<sub>2</sub>. (a) Identifications of multilayer (ML) WS<sub>2</sub> nanosheets beyond the supertwisted spiral WS<sub>2</sub>, which have been named 1<sup>st</sup> to 5<sup>th</sup> from the thinnest to the thickest layers, respectively. The circles represent the excitation areas. (b-f) PL spectra of the first five successive layers (1<sup>B</sup> to 5<sup>B</sup>) in the bottom petal of the supertwisted spiral WS<sub>2</sub>. All the spectral profiles are deconvoluted into two peaks (blue shade for neutral exciton, X<sup>0</sup>, and orange shade for charged exciton, X<sup>-</sup>) using Gauss curves. The dashed lines at 1.99 eV are provided to guide the eye. Photon energy (g), the full width at half maximum (FWHM) (h), integral intensity (i), and spectral weight (j) of X<sup>0</sup> and X<sup>-</sup> of both the supertwisted spiral WS<sub>2</sub> and other multilayers WS<sub>2</sub> as a function of layer index. The hollow squares and circles represent the neutral and charged exciton in the supertwisted spiral WS<sub>2</sub>, while the solid squares and balls represent those in the multilayer WS<sub>2</sub>. The solid line in (i) is a linear fit. (k-o) PL spectra of five-kind multilayer WS<sub>2</sub> highlighted in Fig. 2(a). The five layers are named 1<sup>st</sup> to 5<sup>th</sup>, respectively, from the thinnest to the thickest layer. All the spectral profiles are deconvoluted into two peaks using Gauss curves as well.

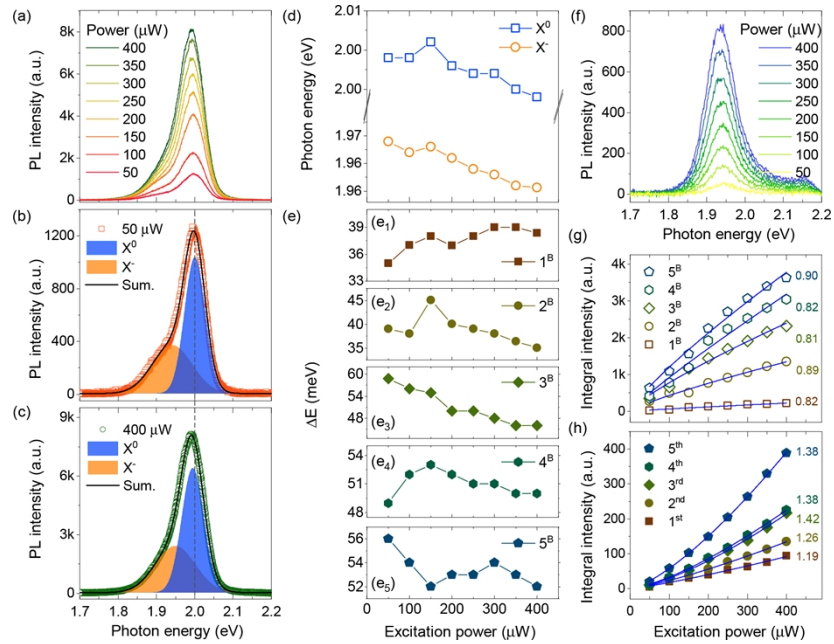


**Fig. 3.** Power-dependent PL spectra of the supertwisted spiral  $\text{WS}_2$ . (a) Power-dependent PL spectra of the  $2^{\text{B}}$  layer. (b, c) Representative PL spectral analysis using two Gauss curves. The dashed lines at 2.0 eV are provided to guide the eye. (d) The power-dependent photon energies of  $X^0$  and  $X^-$  of the  $2^{\text{B}}$  layer in the supertwisted spiral  $\text{WS}_2$ . (e) Power-dependent trion dissociation energy  $\Delta E$  of the five layers for the bottom petal in the supertwisted spiral  $\text{WS}_2$ . (f) Power-dependent PL spectra of the  $2^{\text{nd}}$  multilayer  $\text{WS}_2$ . (g, h) Power-dependent integral PL intensities ( $I$ ) of the supertwisted spiral  $\text{WS}_2$  and conventional multilayer  $\text{WS}_2$ , respectively. The solid lines are the power-law fits with the equation  $I = a \times P^n$ , where  $P$  represents the excitation power. The power exponents  $n$  for each case have been marked in the figure.

cumulative of each successive layer, resulting in enhanced PL intensity and linear increase behavior. Similar to the bottom petal, the photon energy of the two excitons as a function of layer thickness presents subtle shifts, as shown in Fig. 4(d). Beyond PL enhancement, another novel phenomenon is that the power exponents of the multilayer  $\text{WS}_2$  are more significant than 1, while these of the supertwisted spiral  $\text{WS}_2$  are smaller than 1, as illustrated in Fig. 1(e). We speculate that the big power exponents indicate the strong interlayer coupling and the possible nonlinear effect in the conventional multilayer  $\text{WS}_2$ . In contrast, the relatively small power exponents in the supertwisted spiral  $\text{WS}_2$  further reveal the enlarged interlayer spacing and the interlayer decoupling. From this conclusion, we can derive that the spiral structure with different thicknesses (*i.e.*, for different layers) may share the same band structure and thus the similar photon energies of PL emissions, which has been evidenced by their PL spectra, as illustrated in Fig. 2(h). Furthermore, the misalignment between 2D lattices in different layers always emerges in the supertwisted spiral structure, which should contribute to the band structure of diverse layers as well. However, non-interlayer excitons and energy difference have been observed in this experiment, possibly due to the weak interlayer coupling. To explore all these phenomena entirely, the ultimate mechanism resulting in the enlarged interlayer spacing of the supertwisted spiral  $\text{WS}_2$  might require further investigation.

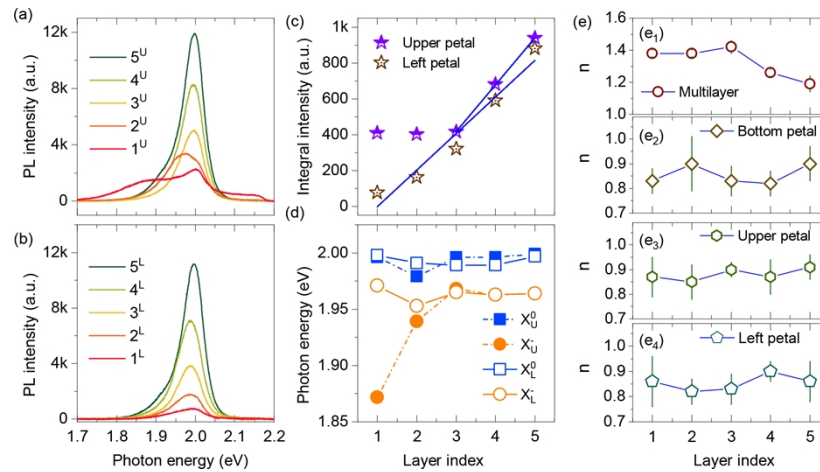


**Fig. 4.** The universality of the anomalous layer-dependent PL spectra in the supertwisted spiral WS<sub>2</sub>. (a, b) Layer-dependent PL spectra of the upper and left petals (abbreviated as U and L), respectively. (c, d) Layer-dependent integral PL intensities and photon energies of the neutral (X<sup>0</sup>) and charged excitons (X<sup>-</sup>) of the upper and left petals, respectively. The solid lines in c are the linear fits. (e) Layer-dependent power exponents of the conventional multilayer WS<sub>2</sub> and the supertwisted spiral WS<sub>2</sub>, respectively.

#### 4. Conclusion

In conclusion, we have investigated the PL spectra of the supertwisted spiral WS<sub>2</sub> and demonstrated the anomalous layer-dependent PL feature that the integral PL intensity of the spiral WS<sub>2</sub> almost linearly increases with the increasing of the layer thickness, rather than significantly decays for the conventional WS<sub>2</sub> as reported in the previous works. Although the underlying mechanism of this phenomenon remains unclear, we tentatively attribute the anomalous layer-dependent PL enhancement to the enlarged interlayer spacing and the decoupling interlayer interaction in the supertwisted spiral WS<sub>2</sub>. Thus, the total PL intensity of the thick layers can be understood as the cumulative of each successive layer. We also performed power-dependent PL spectra and determined the varied dissociation energy of the charged excitons as a function of the excitation power. Compared to the conventional multilayer WS<sub>2</sub> with power exponents bigger than 1, the relatively minor power exponents in the supertwisted spiral WS<sub>2</sub> further hint their decoupling interlayer interaction. Our findings not only reveal the novel PL spectra in the supertwisted spiral WS<sub>2</sub> but also offer a facile and versatile platform for exploring low-dimensional physics and fabricating layered optical and optoelectric devices without considering the rapidly decaying PL intensity in the multilayer TMDCs.

**Funding.** National Key Research and Development Program of China (Grant No. 2022YFA1404201); National Natural Science Foundation of China (Nos. U22A2091, 62222509, 62127817, 62075120, 62075122, 62205187, 62105193, 6191101445, 52273252); Shanxi Province Science and Technology Innovation Talent Team (No. 202204051001014); 111 Project (No. D18001).

**Acknowledgments.** C. Q., X. F., and M. Q. designed and supervised the experiments. M. Q., and X. L. carried out the optical experiments. M. Q., S. W., and T. T. prepared and characterized the sample. G. Z., Z. Y., and J. H. contributed to the data analysis. R. C., G. Z., and S. J. was responsible for instruments managing. M. Q., and C. Q. wrote the manuscript. All authors commented on the manuscript.

**Disclosures.** The authors declare no competing financial interests.

**Data availability.** Data underlying the results presented in this paper are not publicly available at this time but may be obtained from the authors upon reasonable request.



**Supplemental document.** See [Supplement 1](#) for supporting content.

## References

1. Q. H. Wang, K. Kalantar-Zadeh, A. Kis, *et al.*, “Electronics and optoelectronics of two-dimensional transition metal dichalcogenides,” *Nat. Nanotechnol.* **7**(11), 699–712 (2012).
2. M. Xu, T. Liang, M. Shi, *et al.*, “Graphene-like two-dimensional materials,” *Chem. Rev.* **113**(5), 3766–3798 (2013).
3. Y. Lin, X. Ling, L. Yu, *et al.*, “Dielectric screening of excitons and trions in single-layer MoS<sub>2</sub>,” *Nano Lett.* **14**(10), 5569–5576 (2014).
4. S. Mouri, Y. Miyauchi, and K. Matsuda, “Tunable photoluminescence of monolayer MoS<sub>2</sub> via chemical doping,” *Nano Lett.* **13**(12), 5944–5948 (2013).
5. Z. Li, Y. Xiao, Y. Gong, *et al.*, “Active light control of the MoS<sub>2</sub> monolayer exciton binding energy,” *ACS Nano* **9**(10), 10158–10164 (2015).
6. X. Liang, C. Qin, Y. Gao, *et al.*, “Reversible engineering of spin-orbit splitting in monolayer MoS<sub>2</sub> via laser irradiation under controlled gas atmospheres,” *Nanoscale* **13**(19), 8966–8975 (2021).
7. X. Xu, W. Yao, D. Xiao, *et al.*, “Spin and pseudospins in layered transition metal dichalcogenides,” *Nat. Phys.* **10**(5), 343–350 (2014).
8. B. Radisavljevic, A. Radenovic, J. Brivio, *et al.*, “Single-layer MoS<sub>2</sub> transistors,” *Nat. Nanotechnol.* **6**(3), 147–150 (2011).
9. O. Lopez-Sanchez, D. Lembke, M. Kayci, *et al.*, “Ultrasensitive photodetectors based on monolayer MoS<sub>2</sub>,” *Nat. Nanotechnol.* **8**(7), 497–501 (2013).
10. O. Salehzadeh, N. H. Tran, X. Liu, *et al.*, “Exciton kinetics, quantum efficiency, and efficiency droop of monolayer MoS<sub>2</sub> light-emitting devices,” *Nano Lett.* **14**(7), 4125–4130 (2014).
11. M. Bernardi, M. Palummo, and J. C. Grossman, “Extraordinary sunlight absorption and one nanometer thick photovoltaics using two-dimensional monolayer materials,” *Nano Lett.* **13**(8), 3664–3670 (2013).
12. K. F. Mak, C. Lee, J. Hone, *et al.*, “Atomically thin MoS<sub>2</sub>: a new direct-gap semiconductor,” *Phys. Rev. Lett.* **105**(13), 136805 (2010).
13. A. Chaves, J. G. Azadani, H. Alsalman, *et al.*, “Bandgap engineering of two-dimensional semiconductor materials,” *npj 2D Mater. Appl.* **4**(1), 29 (2020).
14. C. Lu, M. Luo, Y. Ge, *et al.*, “Layer-dependent nonlinear optical properties of WS<sub>2</sub>, MoS<sub>2</sub>, and Bi<sub>2</sub>S<sub>3</sub> films synthesized by chemical vapor deposition,” *ACS Appl. Mater. Interfaces* **14**(1), 2390–2400 (2022).
15. Q. Guo, X.-Z. Qi, L. Zhang, *et al.*, “Ultrathin quantum light source with van der Waals NbOCl<sub>2</sub> crystal,” *Nature* **613**(7942), 53–59 (2023).
16. L. Huang, A. Krasnok, A. Alú, *et al.*, “Enhanced light–matter interaction in two-dimensional transition metal dichalcogenides,” *Rep. Prog. Phys.* **85**(4), 046401 (2022).
17. J. D. Lin, C. Han, F. Wang, *et al.*, “Electron-doping-enhanced trion formation in monolayer molybdenum disulfide functionalized with cesium carbonate,” *ACS Nano* **8**(5), 5323–5329 (2014).
18. S. Andleeb, A. Kumar Singh, and J. Eom, “Chemical doping of MoS<sub>2</sub> multilayer by p-toluene sulfonic acid,” *Sci. Technol. Adv. Mater.* **16**(3), 035009 (2015).
19. P. K. Chow, R. B. Jacobs-Gedrim, J. Gao, *et al.*, “Defect-induced photoluminescence in monolayer semiconducting transition metal dichalcogenides,” *ACS Nano* **9**(2), 1520–1527 (2015).
20. H. Wang, C. Zhang, and F. Rana, “Ultrafast dynamics of defect-assisted electron-hole recombination in monolayer MoS<sub>2</sub>,” *Nano Lett.* **15**(1), 339–345 (2015).
21. H. S. Lee, M. S. Kim, Y. Jin, *et al.*, “Efficient exciton-plasmon conversion in Ag nanowire/monolayer MoS<sub>2</sub> hybrids: direct imaging and quantitative estimation of plasmon coupling and propagation,” *Adv. Opt. Mater.* **3**(7), 943–947 (2015).
22. S. Butun, S. Tongay, and K. Aydin, “Enhanced light emission from large-area monolayer MoS<sub>2</sub> using plasmonic nanodisc arrays,” *Nano Lett.* **15**(4), 2700–2704 (2015).
23. X. Fan, Y. Zhao, W. Zheng, *et al.*, “Controllable growth and formation mechanisms of dislocated WS<sub>2</sub> spirals,” *Nano Lett.* **18**(6), 3885–3892 (2018).
24. D. Ouyang, X. Tong, S. Liu, *et al.*, “Superior nonlinear optical response in non-centrosymmetric stacking edge-rich spiral MoTe<sub>2</sub> nanopyramids,” *Adv. Funct. Mater.* **32**, 1 (2022).
25. L. Zhang, K. Liu, A. B. Wong, *et al.*, “Three-dimensional spirals of atomic layered MoS<sub>2</sub>,” *Nano Lett.* **14**(11), 6418–6423 (2014).
26. X. Fan, Y. Jiang, X. Zhuang, *et al.*, “Broken symmetry induced strong nonlinear optical effects in spiral WS<sub>2</sub> nanosheets,” *ACS Nano* **11**(5), 4892–4898 (2017).
27. X. Fan, Z. Ji, R. Fei, *et al.*, “Mechanism of extreme optical nonlinearities in spiral WS<sub>2</sub> above the bandgap,” *Nano Lett.* **20**(4), 2667–2673 (2020).
28. K. F. Mak, K. He, J. Shan, *et al.*, “Control of valley polarization in monolayer MoS<sub>2</sub> by optical helicity,” *Nat. Nanotechnol.* **7**(8), 494–498 (2012).
29. M. J. Shearer, L. Samad, Y. Zhang, *et al.*, “Complex and noncentrosymmetric stacking of layered metal dichalcogenide materials created by screw dislocations,” *J. Am. Chem. Soc.* **139**(9), 3496–3504 (2017).
30. Y. Zhang, Y. Lee, W. Zhang, *et al.*, “Deterministic fabrication of twisted Van Der Waals structures,” *Adv. Funct. Mater.* **33**(23), 2212210 (2023).

31. Y. Zhao and S. Jin, "Stacking and twisting of layered materials enabled by screw dislocations and non-euclidean surfaces," *Acc. Mater. Res.* **3**(3), 369–378 (2022).
32. P. Ci, Y. Zhao, M. Sun, *et al.*, "Breaking rotational symmetry in supertwisted WS<sub>2</sub> spirals via Moiré magnification of intrinsic heterostrain," *Nano Lett.* **22**(22), 9027–9035 (2022).
33. K. B. Simbulan, T.-D. Huang, G.-H. Peng, *et al.*, "Selective photoexcitation of finite-momentum excitons in monolayer MoS<sub>2</sub> by twisted light," *ACS Nano* **15**(2), 3481–3489 (2021).
34. J. Zhou, J. Cui, S. Du, *et al.*, "A natural indirect-to-direct band gap transition in artificially fabricated MoS<sub>2</sub> and MoSe<sub>2</sub> flowers," *Nanoscale* **15**(17), 7792–7802 (2023).
35. H. Su, C. Wei, A. Deng, *et al.*, "Anomalous enhancement of valley polarization in multilayer WS<sub>2</sub> at room temperature," *Nanoscale* **9**(16), 5148–5154 (2017).
36. A. Berkdemir, H. R. Gutiérrez, A. R. Botello-Méndez, *et al.*, "Identification of individual and few layers of WS<sub>2</sub> using Raman spectroscopy," *Sci. Rep.* **3**(1), 1755 (2013).
37. S. B. Desai, G. Seol, J. S. Kang, *et al.*, "Strain-induced indirect to direct bandgap transition in multilayer WSe<sub>2</sub>," *Nano Lett.* **14**(8), 4592–4597 (2014).
38. Y. Li, X. Li, T. Yu, *et al.*, "Accurate identification of layer number for few-layer WS<sub>2</sub> and WSe<sub>2</sub> via spectroscopic study," *Nanotechnology* **29**(12), 124001 (2018).
39. Z. He, Y. Sheng, Y. Rong, *et al.*, "Layer-dependent modulation of tungsten disulfide photoluminescence by lateral electric fields," *ACS Nano* **9**(3), 2740–2748 (2015).
40. C. Gao, S. You, Y. Zhang, *et al.*, "Strong coupling between excitons and quasi-bound states in the continuum mode with stable resonance wavelength in the near-infrared region," *Appl. Phys. Lett.* **124**(1), 1 (2024).
41. J. C. Reed, A. Y. Zhu, H. Zhu, *et al.*, "Wavelength tunable microdisk cavity light source with a chemically enhanced MoS<sub>2</sub> emitter," *Nano Lett.* **15**(3), 1967–1971 (2015).
42. S. Wu, S. Buckley, J. R. Schaibley, *et al.*, "Monolayer semiconductor nanocavity lasers with ultralow thresholds," *Nature* **520**(7545), 69–72 (2015).
43. M. Buscema, G. A. Steele, H. S. J. van der Zant, *et al.*, "The effect of the substrate on the Raman and photoluminescence emission of single-layer MoS<sub>2</sub>," *Nano Res.* **7**(4), 561–571 (2014).
44. X. Fan, W. Zheng, H. Liu, *et al.*, "Nonlinear photoluminescence in monolayer WS<sub>2</sub>: parabolic emission and excitation fluence-dependent recombination dynamics," *Nanoscale* **9**(21), 7235–7241 (2017).
45. C. Yang, Y. Gao, C. Qin, *et al.*, "All-optical reversible manipulation of exciton and trion emissions in monolayer WS<sub>2</sub>," *Nanomaterials* **10**(1), 23 (2020).